Forces between Cylindrical Nanoparticles in a Liquid Crystal†

David L. Cheung and Michael P. Allen*

Department of Physics and Centre for Scientific Computing, University of Warwick, Coventry, CV4 7AL, United Kingdom

Received August 2, 2007. In Final Form: October 21, 2007

Using classical density functional theory, the forces between two cylindrical nanoparticles in a liquid crystal solvent are calculated. Both the nematic and isotropic phases of the solvent are considered. In the nematic phase, the interaction is highly anisotropic. At short range, changes in the defect structure around the cylinders leads to a complex interaction between them. In the isotropic phase, an attractive interaction arises due to overlap between halos of ordered fluid adsorbed on the surfaces of the cylinders.

1. Introduction

Composites of solid particles dispersed in liquid crystals form a class of novel materials with a wide range of phenomenology.[1] The spontaneous ordering of the liquid crystal (LC) molecules allows manipulation of the orientations[2,3] and positions[4] of the nanoparticles. This gives rise to a number of current and potential applications for these, such as in displays[5] or materials processing.[2] Interactions between LCs and nanoparticles are also important in other applications of liquid crystals, such as biosensors.[6]

Elastic distortions of the liquid crystal director play an important role in the physics of LC−nanoparticle composites. Depending on the anchoring strength and direction at the nanoparticle surface, a range of different director configurations,[7] which often contain topological defects (disclinations), may exist in its vicinity. This elastic distortion gives rise to long-ranged, solvent-mediated interactions between nanoparticles in LCs, leading to structures such as colloidal chains[8] or crystals[9] ordered over many micrometers. There has been much interest in studying the behavior of LC−nanoparticle composites, for both ordered and disordered phases of the LC. At temperatures above the nematic−isotropic (NI) transition of the LC solvent ($T > T_{NI}$), a layer of ordered (paranematic) fluid is often adsorbed on the nanoparticle surface. Overlap between these layers leads to a strong attraction between nanoparticles and hence to flocculation in LC−colloid dispersions close to T_{NI}.

In previous work, classical density functional theory (DFT) has been applied to the study of LC−nanoparticle composites.[10,11] This has proven to give results in agreement with both molecular simulations and phenomenological theories, while being less computationally expensive than the former and retaining a direct link to molecular structure lacking in the latter. In this paper, attention is turned to the interaction between two parallel cylindrical nanoparticles in both nematic and isotropic LCs. When the anchoring on the particle surface is normal (homeotropic), two line defects, disclinations of strength 1/2, appear on either side of the particle. At large separations, this defect structure gives rise to a quadrupolar effective interaction between the cylinders.[12] As the separation is decreased, changes in the defect structure around the cylinders lead to a more complex interaction. Examining this short-range interaction is a key aim of this paper. This work will also examine the solvent-induced interaction between cylinders in the isotropic phase of the solvent, which is largely due to the overlap between the halos of ordered fluid on the cylinders' surfaces.

2. Theory

The liquid crystal solvent is modeled as a fluid of axially symmetric hard ellipsoids of aspect ratio $e = a/b = 15$ (in the rest of this paper, $b = 1$, the minor axis, will be taken to be the unit of length). The grand potential of such a system may be written as[13]

$$\beta\,\Omega[\rho] = \beta\,F_{id}[\rho] + \beta\,F_{ex}[\rho] + \beta \int \mathrm{d}\boldsymbol{r}\,\mathrm{d}\boldsymbol{u}\;\rho(\boldsymbol{r},\boldsymbol{u})\,(V_{ext}(\boldsymbol{r},\boldsymbol{u}) - \mu) \quad (1)$$

Here, $\rho \equiv \rho(\boldsymbol{r}, \boldsymbol{u})$ is the single-particle density, which depends on the particle position vector $\boldsymbol{r}$ and orientation vector $\boldsymbol{u}$. $V_{ext}(\boldsymbol{r}, \boldsymbol{u})$ is the external potential, μ is the chemical potential, and $\beta = 1/k_BT$. $F_{id}[\rho]$ and $F_{ex}[\rho]$ are the ideal and excess free energy functionals, respectively. The ideal free energy is given by

$$\beta\,F_{id}[\rho] = \int \mathrm{d}\boldsymbol{r}\,\mathrm{d}\boldsymbol{u}\;\rho(\boldsymbol{r},\boldsymbol{u})\,(\log\rho(\boldsymbol{r},\boldsymbol{u}) - 1) \quad (2)$$

The exact form of the excess free energy is generally unknown. Here, we employ the Onsager approximation[14]

$$\beta\,F_{ex}[\rho] = -\frac{1}{2}\int \mathrm{d}\boldsymbol{r}_1\,\mathrm{d}\boldsymbol{r}_2\,\mathrm{d}\boldsymbol{u}_1\,\mathrm{d}\boldsymbol{u}_2\,f(\boldsymbol{r}_{12},\boldsymbol{u}_1,\boldsymbol{u}_2)\,\rho(\boldsymbol{r}_1,\boldsymbol{u}_1)\rho(\boldsymbol{r}_2,\boldsymbol{u}_2) \quad (3)$$

where $\boldsymbol{r}_{12} = \boldsymbol{r}_1 - \boldsymbol{r}_2$ and $f(\boldsymbol{r}_{12}, \boldsymbol{u}_1, \boldsymbol{u}_2) = \exp\{-\beta V(\boldsymbol{r}_{12}, \boldsymbol{u}_1, \boldsymbol{u}_2)\} - 1$ is the Mayer function. $V(\boldsymbol{r}_{12}, \boldsymbol{u}_1, \boldsymbol{u}_2)$ is the intermolecular potential, which in the present work is the hard ellipsoid potential that is ∞ when two molecules overlap ($f(\boldsymbol{r}_{12}, \boldsymbol{u}_1, \boldsymbol{u}_2) = -1$) and 0 otherwise ($f(\boldsymbol{r}_{12}, \boldsymbol{u}_1, \boldsymbol{u}_2) = 0$). Equation 3 corresponds to

† Part of the Molecular and Surface Forces special issue.

(1) Stark, H. *Phys. Rep.* **2001**, *351*, 387−474.
(2) Lynch, M.; Patrick, D. *Nano Lett.* **2002**, *2*, 1197−1201.
(3) Mitov, M.; Portet, C.; Bourgerette, C.; Snoeck, E.; Verelst, M. *Nat. Mater.* **2002**, *1*, 229−231.
(4) Dabbs, D. M.; Aksay, I. A. *Annu. Rev. Phys. Chem.* **2000**, *51*, 601−622.
(5) Sikharulidze, D. *Appl. Phys. Lett.* **2005**, *86*, 033507/1.
(6) Gupta, V. K.; Skaife, J. J.; Dubrovsky, T. B.; Abbott, N. L. *Science* **1998**, *279*, 2077−2080.
(7) Ruhwandl, R. W.; Terentjev, E. M. *Phys. Rev. E* **1997**, *56*, 5561−5565.
(8) Poulin, P. *Curr. Opin. Colloid Interface Sci.* **1999**, *4*, 66−71.
(9) Muševic, I.; Škarabot, M.; Tkalec, U.; Ravnik, M.; Žumer, S. *Science* **2006**, *313*, 954−958.
(10) Cheung, D. L.; Allen, M. P. *Phys. Rev. E* **2006**, *74*, 021701/1−8.
(11) Cheung, D. L.; Allen, M. P. *Phys. Rev. E* **2007**, *76*, 041706/1-7.
(12) Tasinkevych, M.; Silvestre, N. M.; Patrício, P.; Telo da Gama, M. M. *Eur. Phys. J. E* **2002**, *9*, 341−347.
(13) Hansen, J.-P.; McDonald, I. R. *Theory of Simple Liquids*, 2nd ed.; Academic Press: London, 1986.
(14) Onsager, L. *Ann. N. Y. Acad. Sci.* **1949**, *51*, 627.

10.1021/la702348c CCC: $40.75
Published on Web 01/08/2008

truncating the virial expansion after the pair term. While Onsager theory is only exact in the limit of infinite elongation, previous studies have shown it to be in good agreement with simulations for molecules of the elongation under consideration here.[15,16]

The interaction between a fluid molecule located at $\boldsymbol{r} = (x, y, z)$ and a cylindrical nanoparticle of radius R, whose axis is oriented along y and located at $\boldsymbol{S}_1 = (X_1, Z_1)$ in the xz-plane, is independent of the y-coordinates and may be written as

$$V_{\text{ext}}^{(1)}(\boldsymbol{s}) = \begin{cases} V_0 \tanh(b/w) & |\boldsymbol{s} - \boldsymbol{S}_1| - R < -b \\ \frac{1}{2}V_0\left[\tanh\left(\frac{R - |\boldsymbol{s} - \boldsymbol{S}_1|}{w}\right) + \tanh(b/w)\right] & ||\boldsymbol{s} - \boldsymbol{S}_1| - R| < b \\ 0 & |\boldsymbol{s} - \boldsymbol{S}_1| - R > b \end{cases} \quad (4)$$

where $\boldsymbol{s} = (x, z)$, $V_0 = 50k_BT$, and $w = b/5$. The nanoparticle radius is $R = 15b$. This represents a sharply varying repulsive potential acting on the ellipsoid centers of mass; it excludes the centers of the molecules from the cylinder and gives rise to homeotropic (normal) anchoring at the surface. This allows half of the ellipsoid volume of each fluid molecule to penetrate inside the cylindrical nanoparticle: the aim is to mimic the effect of a semipermeable surface coating, such as a polymer brush, applied to an impermeable cylinder, such as a carbon nanotube[2] of smaller radius. Note that, in this case, the potential V_{ext} does not depend explicitly on the ellipsoid orientation vector $\boldsymbol{u}$; by making V_{ext} depend on $\boldsymbol{u}$, other anchoring conditions are easily generated. In this work, the external potential is a sum of two terms $V_{\text{ext}} = V_{\text{ext}}^{(1)} + V_{\text{ext}}^{(2)}$ from cylinders located at, respectively, $\boldsymbol{S}_1$ and $\boldsymbol{S}_2$.

It should be noted that the cylinder−particle interaction is, for practical purposes, a hard repulsive potential acting solely on the ellipsoid particle centers, without an explicit orientation-dependence. The results should not depend sensitively on the values of V_0 and w. The homeotropic anchoring arises from entropic effects, that is, the packing of ellipsoids in the most efficient manner on the surface. This anchoring condition has been investigated quantitatively before for a planar hard surface and for ellipsoids identical to the ones studied here.[16,17] The effective extrapolation length, which measures the anchoring strength, depends, of course, on the fluid density, but it is of the order of the length of a molecule. This corresponds to "strong anchoring'' in the conventional terminology. By using a repulsion of finite (but very large) height and slightly softened form, we avoid some numerical difficulties in the minimization of the free energy.

To make the calculations computationally tractable, the angularly dependent functions are expanded in spherical harmonics[10,11]

$$\log \rho(\boldsymbol{r}, \boldsymbol{u}) = \sum_{l,m} \tilde{\rho}_{lm}(\boldsymbol{s})\, Y_{lm}(\boldsymbol{u}) \quad (5a)$$

$$\rho(\boldsymbol{r}, \boldsymbol{u}) = \sum_{l,m} \rho_{lm}(\boldsymbol{s})\, Y_{lm}^*(\boldsymbol{u}) \quad (5b)$$

$$V_{\text{ext}}(\boldsymbol{r}, \boldsymbol{u}) = \sum_{l,m} V_{lm}(\boldsymbol{s})\, Y_{lm}(\boldsymbol{u}) \quad (5c)$$

where translational invariance along the y-direction allows us to write the coefficients as functions of $\boldsymbol{s}$. The indices range over integer values $l = 0, 1, 2...$ and $m = 0, \pm1, ..., \pm l$. The Mayer function is expanded as[18]

$$f(\boldsymbol{r}_{12}, \boldsymbol{u}_1, \boldsymbol{u}_2) = \sum_{l_1,l_2,l} f_{l_1l_2l}(r_{12})\, \Phi_{l_1l_2l}(\boldsymbol{u}_1, \boldsymbol{u}_2, \hat{\boldsymbol{r}}_{12}) \quad (6)$$

where $r_{12} = |\boldsymbol{r}_{12}|, \hat{\boldsymbol{r}}_{12} = \boldsymbol{r}_{12}/r_{12}$. In this equation, $\Phi_{l_1l_2l}$ is a rotational invariant[19]

$$\Phi_{l_1l_2l}(\boldsymbol{u}_1, \boldsymbol{u}_2, \hat{\boldsymbol{r}}_{12}) = 4\pi \sum_{m_1,m_2,m} \begin{pmatrix} l_1 & l_2 & l \\ m_1 & m_2 & m \end{pmatrix} Y_{l_1m_1}(\boldsymbol{u}_1)\, Y_{l_2m_2}(\boldsymbol{u}_2)\, C_{lm}(\hat{\boldsymbol{r}}_{12})$$

where $\begin{pmatrix} l_1 & l_2 & l \\ m_1 & m_2 & m \end{pmatrix}$ is the standard 3j-symbol and $C_{lm} = (4\pi/(2l + 1))^{1/2}Y_{lm}$. Inserting the expansions into eq 1, and integrating over angles and the y-direction, gives the grand potential (per unit length along the y-direction denoted as L)

$$\frac{\beta\,\Omega[\rho]}{L} = \int \mathrm{d}\boldsymbol{s} \sum_{l,m} \rho_{lm}(\boldsymbol{s})\,(\tilde{\rho}_{lm}(\boldsymbol{s}) - \sqrt{4\pi}(1 + \beta\mu)\delta_{l0} + \beta\, V_{lm}(\boldsymbol{s})) + \int \mathrm{d}\boldsymbol{s}_1\, \mathrm{d}\boldsymbol{s}_2 \sum_{\substack{l_1,m_1 \\ l_2,m_2}} \mathscr{C}_{l_1m_1l_2m_2}(\boldsymbol{s}_{12})\, \rho_{l_1m_1}(\boldsymbol{s}_1)\, \rho_{l_2m_2}(\boldsymbol{s}_2) \quad (7)$$

where the Kronecker delta $\delta_{l0} = 1$ when $l = 0$ and $\delta_{l0} = 0$ otherwise. The quantities $\mathscr{C}_{l_1m_1l_2m_2}(\boldsymbol{s}_{12})$ come from integrating the Mayer function and are the spherical harmonic coefficients of the excluded length (in the y-direction) of two molecules with a separation vector $\boldsymbol{s}_{12} = \boldsymbol{s}_1 - \boldsymbol{s}_2$ in the xz-plane, treated as a function of the molecular orientations. As the last term in eq 7 is a convolution, it is most conveniently evaluated in reciprocal space in the form

$$\sum_{\boldsymbol{k}} \sum_{\substack{l_1,m_1 \\ l_2,m_2}} \mathscr{C}_{l_1m_1l_2m_2}(\boldsymbol{k})\, \rho_{l_1m_1}(\boldsymbol{k})\, \rho_{l_2m_2}(\boldsymbol{k}) \quad (8)$$

where $\rho_{lm}(\boldsymbol{k})$ and $\mathscr{C}_{l_1m_1l_2m_2}(\boldsymbol{k})$ are, respectively, the two-dimensional Fourier transforms of $\rho_{lm}(\boldsymbol{s})$ and $\mathscr{C}_{l_1m_1l_2m_2}(\boldsymbol{s}_{12})$.

To find the equilibrium density, the functions are tabulated on a regular grid in the xz-plane; the grid spacing is $\delta x = \delta z = 0.5b$, with the molecular length corresponding to 30 grid points. A 600 × 600 grid, that is, of side $300b$, with periodic boundaries, was found to be sufficient. The grand potential is then minimized with respect to the $\tilde{\rho}_{lm}(\boldsymbol{s})$ coefficients at each grid point using the conjugate gradient method.[20] When required, the coefficients $\rho_{lm}(\boldsymbol{s})$ are calculated through eq 5, with angular integrations performed using Lebedev quadrature.[21,22]

Once the equilibrium density coefficients $\rho_{lm}(\boldsymbol{s})$ have been determined, the number density $\rho(\boldsymbol{s})$ and order tensor $Q_{\alpha\beta}(\boldsymbol{s})$ may be found from

$$\rho(\boldsymbol{s}) = \int \mathrm{d}\boldsymbol{u}\, \rho(\boldsymbol{s}, \boldsymbol{u}) = \sqrt{4\pi}\, \rho_{00}(\boldsymbol{s}) \quad (9)$$

$$Q_{\alpha\beta}(\boldsymbol{s}) = \frac{3}{2}\int \mathrm{d}\boldsymbol{u}\, \rho(\boldsymbol{s}, \boldsymbol{u})\, u_\alpha(\boldsymbol{s})\, u_\beta(\boldsymbol{s}) - \frac{1}{2}\delta_{\alpha\beta} \qquad \alpha, \beta = x, y, z \quad (10)$$

(15) Camp, P. J.; Mason, C. P.; Allen, M. P.; Khare, A. A.; Kofke, D. A. *J. Chem. Phys.* **1996**, *105*, 2837−2849.
(16) Allen, M. P. *Mol. Phys.* **1999**, *96*, 1391−1397.
(17) Andrienko, D.; Germano, G.; Allen, M. P. *Phys. Rev. E* **2000**, *62*, 6688−6693.
(18) Andrienko, D.; Allen, M. P. *Phys. Rev. E* **2002**, *65*, 021704/1−11.
(19) Gray, C. G.; Gubbins, K. E. *Theory of molecular fluids. 1. Fundamentals*; Clarendon Press: Oxford, U.K., 1984.
(20) Press, W. H.; Flannery, B. P.; Teukolsky, S. A.; Vetterling, W. T. *Numerical Recipes*; Cambridge University Press: Cambridge, U.K., 1986.
(21) Lebedev, V. I. *Zh. Vychisl. Mat. Mat. Fiz* **1976**, *16*, 293 (in Russian, English translation: *J. Comput. Math. Math. Phys.* **1976**, *16* (10)).
(22) Lebedev, V. I. *Sib. Mat. Zh.* **1977**, *18*, 132.

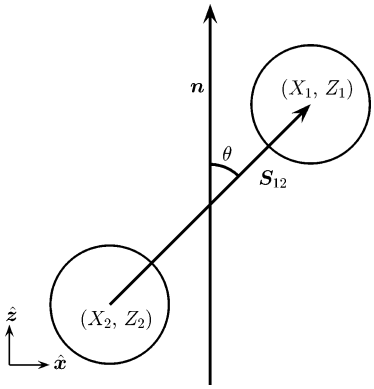

Figure 1. Two-cylinder configuration. The system is translationally invariant in the *y*-direction. The angle θ of the interparticle vector is taken with respect to the far-field director, which defines the *z*-direction.

The spatially varying order parameter $Q(\boldsymbol{s})$ is given by the largest eigenvalue of $Q_{\alpha\beta}(\boldsymbol{s})$, and the director $n(\boldsymbol{s})$ is given by the eigenvector associated with $Q(\boldsymbol{s})$. In the present work, the director is found to lie in the *xz*-plane, and so it may be characterized by an angle $\varphi(\boldsymbol{s})$ such that $\tan\varphi = n_x/n_z$, measuring the deviation from the far-field director, which is taken to lie in the *z*-direction. Calculations were performed on systems containing two cylinders at chemical potentials $\beta\mu = 1.4$ (nematic) and $\beta\mu = 1.2$ (isotropic). For the model and parameters used in this work, $\beta\mu_{NI} \approx 1.31$. The separation $S_{12} = |\boldsymbol{S}_1 - \boldsymbol{S}_2|$ between the cylinders ranged from $S_{12} = 30b$ (contact) to $S_{12} = 150b$; and in the nematic phase, the angle between the director and separation vector was $\theta = 0$, $\pi/6$, $\pi/4$, $\pi/3$, and $\pi/2$. The setup is shown in Figure 1.

It is worth stressing that the director is not constrained to lie perpendicular to the cylinder axes: this configuration arises naturally as the one of lowest free energy, as is the case for a single cylinder with homeotropic anchoring.[23] It would be possible to constrain the far-field director in other directions, but this is not the topic of the present study.

The LC mediated force (per unit length) on the cylinders may be found by differentiating the grand potential with respect to (either one of) the cylinder coordinates[24,25]

$$\frac{\beta\boldsymbol{F}_1}{L} = \int \mathrm{d}\boldsymbol{s}\, \sqrt{4\pi}w^{-1}\, \mathrm{sech}^2\left(\frac{R - |\boldsymbol{s} - \boldsymbol{S}_1|}{w}\right) \rho_{00}(\boldsymbol{s})\, (\boldsymbol{s} - \boldsymbol{S}_1) \quad (11)$$

(similarly for $\boldsymbol{F}_2$) where the integration is over the region $|\boldsymbol{s} - \boldsymbol{S}_1| < R - b$. It is most convenient to resolve the force between the cylinders into a radial component F_r along the separation vector $\boldsymbol{S}_{12}$, and a tangential component F_t perpendicular to $\boldsymbol{S}_{12}$.

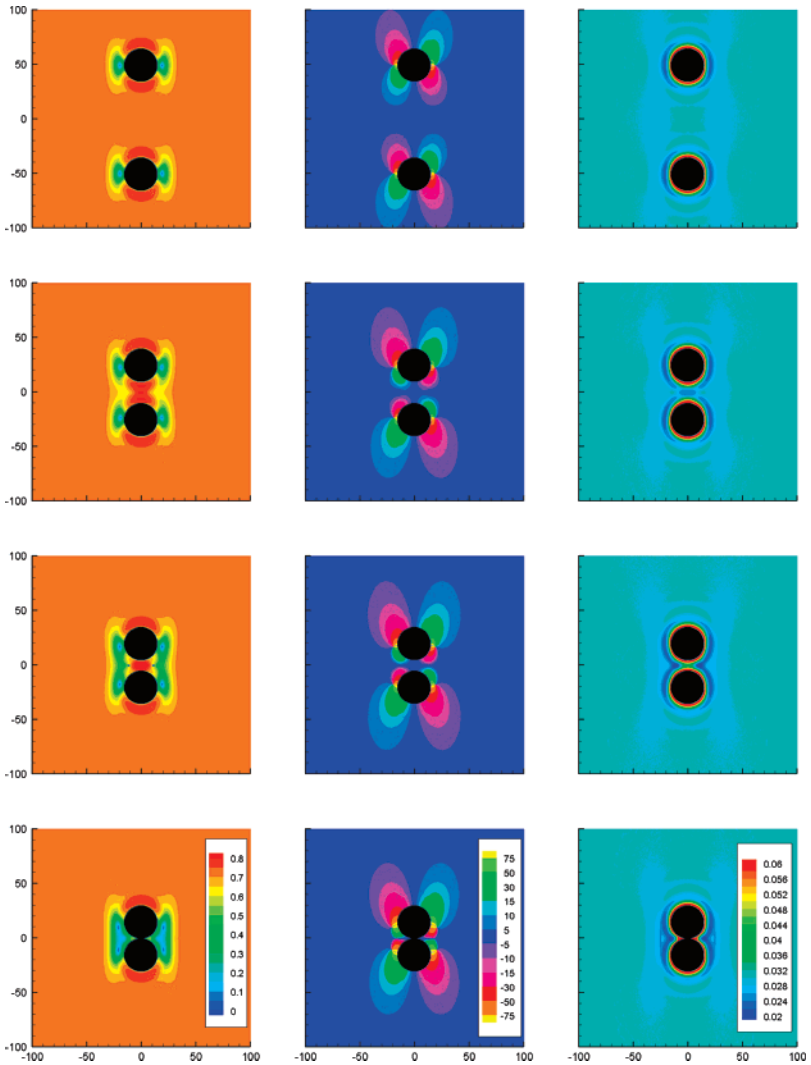

Figure 2. Maps of order parameter $Q(\boldsymbol{s})$ (left), director angle $\varphi(\boldsymbol{s})$ (center), and number density $\rho(\boldsymbol{r})$ (right) of LCs around two cylindrical nanoparticles with $\theta = 0$ in the solvent nematic phase ($\beta\mu = 1.4$). Only the central region $-100 \le x/b, z/b \le 100$ is shown.

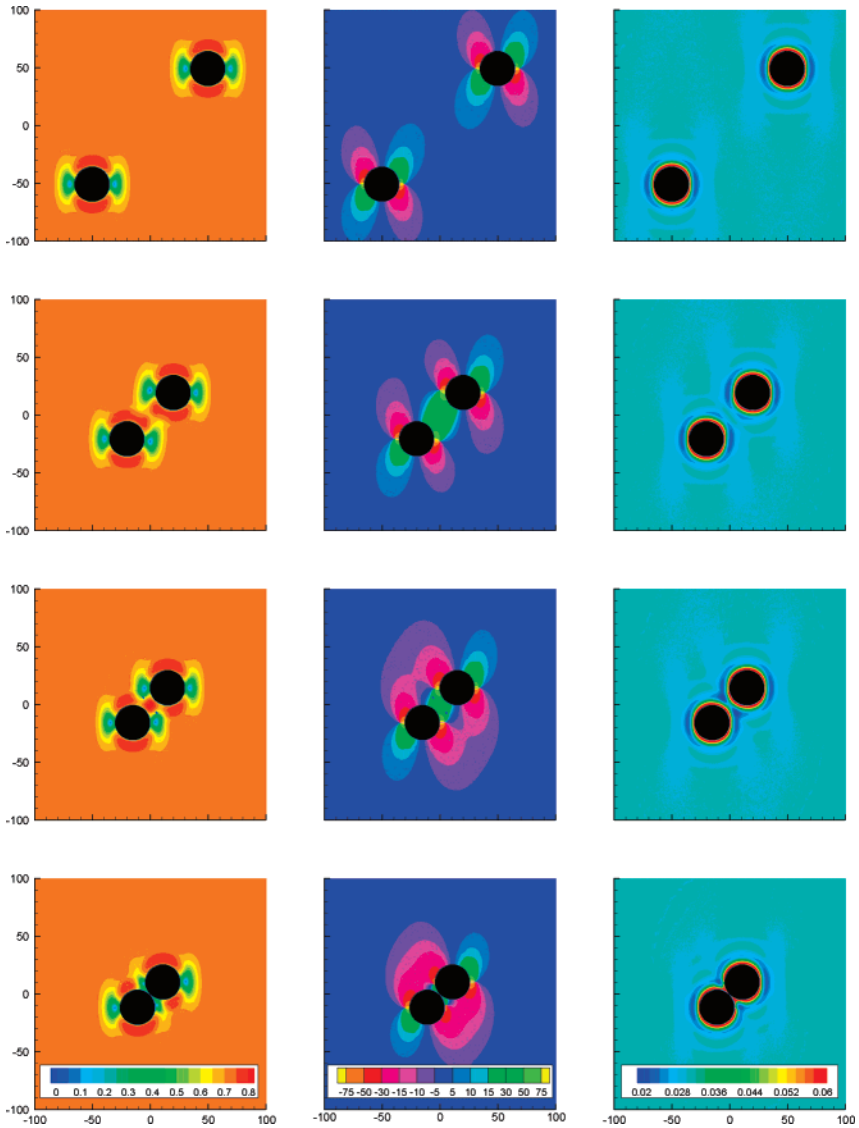

Figure 3. Maps of order parameter $Q(\boldsymbol{s})$ (left), director angle $\varphi(\boldsymbol{s})$ (center), and number density $\rho(\boldsymbol{r})$ (right) of LCs around two cylindrical nanoparticles with $\theta = \pi/4$ in the solvent nematic phase ($\beta\mu = 1.4$). Only the central region $-100 \leq x/b, z/b \leq 100$ is shown.

3. Results

3.1. Nematic Phase. Shown in Figures 2−4 are order parameter and director angle maps for two cylinders in the nematic phase ($\beta\mu = 1.4$) of the solvent. When the separation is large, the structure of the LC fluid around the cylinders is the same as for isolated cylinders: the two strength-1/2 defects are clearly seen both in the reduced value of the order parameter near the disclination lines and in the rotation of the director angle about these lines, which lie at the same values of z as the respective cylinder axes. On decreasing the separation between the cylinders, the structure of the fluid begins to deform, in a manner which varies depending on the angle θ of the separation vector $\boldsymbol{S}_{12}$ relative to the far-field director $\boldsymbol{n}$. When $\theta = 0$ (Figure 2), the fluid structure changes only slightly, with the defects around each particle merging together when the particles get close to contact. This is in contrast to a Landau−de Gennes theory calculation on a 2D nematic system[12] where the defects near the particles twist around but do not merge. When $\theta = \pi/4$ (Figure 3), the local director between the particles rotates to lie along the separation vector. As the particles come into contact, two of the defects shrink in size.

The change in structure is most dramatic for a separation vector $\boldsymbol{S}_{12}$ perpendicular to $\boldsymbol{n}$, $\theta = \pi/2$ (Figure 4). On decreasing separation, the defects between the particles merge and then split along the director. This is in agreement with previous molecular dynamics (MD) simulations[26] and Landau−de Gennes theory.[12] The change in defect structure is also reminiscent of the behavior of spherical nanoparticles with so-called "Saturn ring'' defects.[27−29] On decreasing the separation to contact, these defects decrease in size and move closer to the cylinder surface until they are sitting in the cusps between them.

(23) Andrienko, D.; Allen, M. P.; Skačej, G.; Žumer, S. *Phys. Rev. E* **2002**, *65*, 041702/1−7.
(24) Löwen, H.; Madden, P. A.; Hansen, J.-P. *Phys. Rev. Lett.* **1992**, *68*, 1081−1084.
(25) Löwen, H.; Hansen, J.-P.; Madden, P. A. *J. Chem. Phys.* **1993**, *98*, 3275−3289.
(26) Andrienko, D.; Tasinkevych, M.; Patricio, P.; Allen, M. P.; Telo da Gama, M. M. *Phys. Rev. E* **2003**, *68*, 051702/1−5.
(27) Guzmán, O.; Kim, E. B.; Grollau, S.; Abbott, N. L.; de Pablo, J. J. *Phys. Rev. Lett.* **2003**, *91*, 235507/1−4.
(28) Al-Barwani, M. S.; Sutcliffe, G. S.; Allen, M. P. *J. Phys. Chem. B* **2004**, *108*, 6663−6666.
(29) Kim, E. B.; Guzmăn, O.; Grollau, S.; Abbott, N. L.; de Pablo, J. J. *J. Chem. Phys.* **2004**, *121*, 1949−1961.

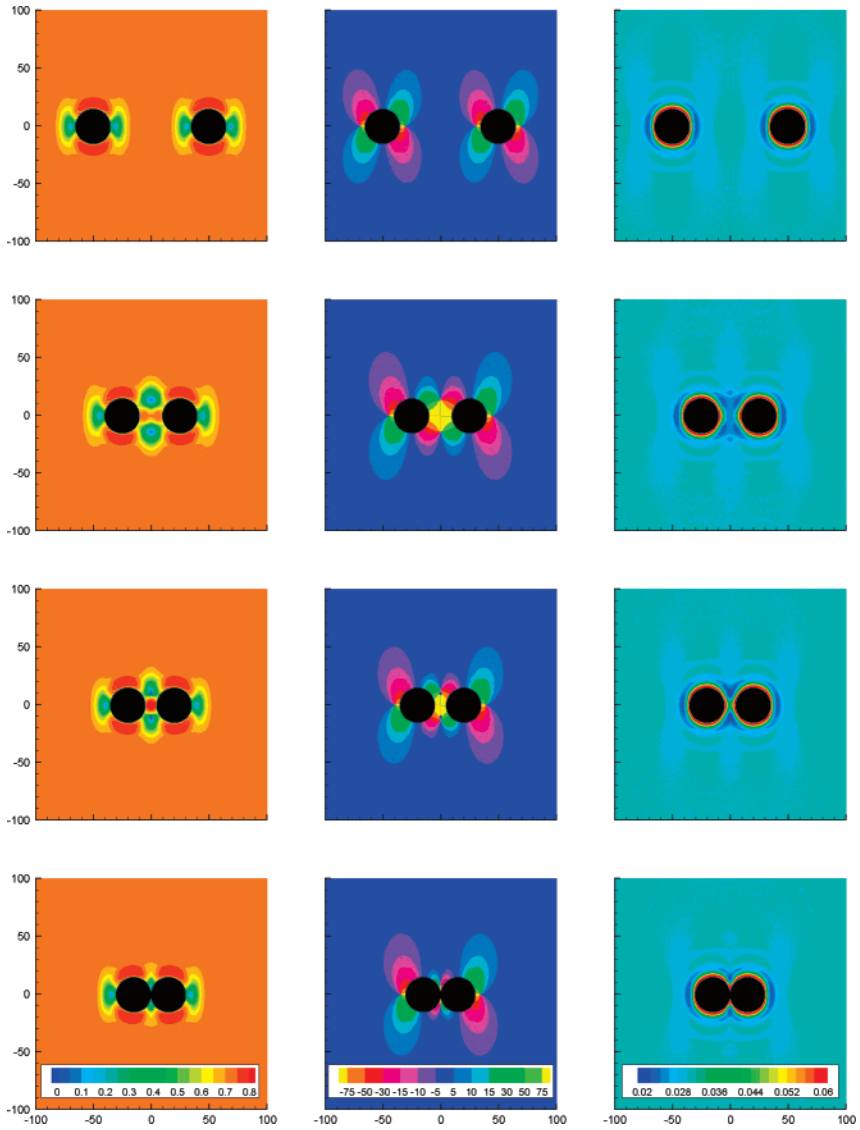

Figure 4. Maps of order parameter $Q(\boldsymbol{s})$ (left), director angle $\varphi(\boldsymbol{s})$ (center), and number density $\rho(\boldsymbol{r})$ (right) of LCs around two cylindrical nanoparticles with $\theta = \pi/2$ in the solvent nematic phase ($\beta\mu = 1.4$). Only the central region $-100 \leq x/b, z/b \leq 100$ is shown.

Plots of the grand potential against separation for a range of angles θ are shown in Figure 5. For all angles, the potential is repulsive at short distances and has a potential well at $S_{12} \approx 33b$. The short-range repulsion is due to the overlap between the high-density regions at the cylinder surface and the elastic distortions due to the normal anchoring at the cylinder surface. This repulsive interaction at short range is indicative of strong normal anchoring on the cylinder surfaces.[12] We note in passing that the form of the ellipsoid−cylinder interaction studied here does not produce a depletion interaction, that is, there is no region between the cylinders from which the ellipsoids are geometrically excluded. For $\theta = 0$, there is a marked potential barrier at larger separations and a repulsive potential extending over 2−3 cylinder diameters. On increasing θ, the potential barrier disappears and the potential becomes attractive at large S_{12}. The range of this interaction is longest for $\theta = \pi/4$ and shortest for $\theta = \pi/2$. The short range of the interaction in this configuration may arise due to the short range of density and order parameter variation perpendicular to the director for isolated cylinders, which in turn is a result of the presence of the defects.[10,23]

The radial and tangential components of the solvent induced force are shown in Figure 6. F_r is dominated by the excluded volume interaction of the adsorbed layers on the cylinders.[26] Except for $\theta = 0$ and $\theta = \pi/2$, there is a nonzero tangential force

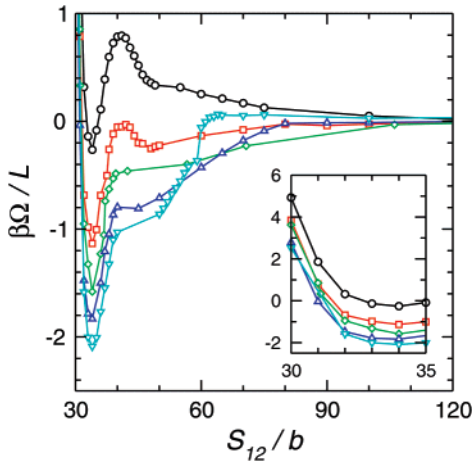

Figure 5. Grand potential (per unit length) against separation for two cylinders in the solvent nematic phase ($\beta\mu = 1.4$) for the following separation angles θ: 0 (circles, black), $\pi/6$ (squares, red), $\pi/4$ (tilted squares, green), $\pi/3$ (up triangles, blue), and $\pi/2$ (down triangles, cyan). The inset shows the strongly repulsive region at low separation.

F_t. In agreement with MD simulations,[26] the magnitude of this component is significantly smaller than that of the radial

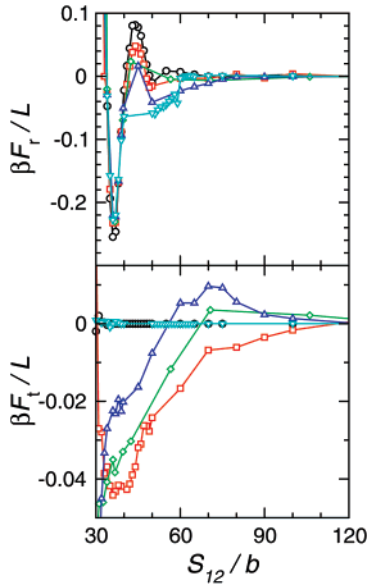

Figure 6. Radial (top) and tangential (bottom) force per unit length against separation for cylinders in the nematic phase of the solvent ($\beta\mu = 1.4$) for the following separation angles θ: 0 (circles, black), $\pi/6$ (squares, red), $\pi/4$ (tilted squares, green), $\pi/3$ (up triangles, blue), and $\pi/2$ (down triangles, cyan).

component. For $\theta = 0$ and $\theta = \pi/2$, DFT predicts $F_t = 0$ due to the symmetry of the fluid structure around the cylinders in this configuration.

3.2. Isotropic Phase. Shown in Figure 7 are order parameter and director angle maps for two cylinders in the isotropic phase of the solvent, at a chemical potential $\beta\mu = 1.2$ quite close to the NI transition. When the particles are far apart, the structure around each is cylindrically symmetrical and is localized to a surface layer. As the cylinders are brought together, a bridge of orientationally ordered fluid appears between them, which leads to an attractive interaction between the cylinders. This interaction causes flocculation of nanoparticles in LCs above T_{NI}. The bridge starts to form when $S_{12} \approx 60b-65b$, which is comparable to the distance at which a nematic bridge is seen to form between a single cylinder and a planar substrate[11] for this chemical potential.

The variation of the grand potential with cylinder separation in the isotropic phase is shown in Figure 8. As in the nematic phase, this is strongly repulsive at small cylinder separations and has an attractive well at $S_{12} \approx 33b$. At larger distances, the potential is attractive and varies approximately linearly with separation. This arises from the nematic bridge that appears between the particles at this state point. Unlike the case of a single cylinder in the vicinity of a planar substrate,[11] there is no abrupt change in the potential, indicating that the bridge forms continuously.

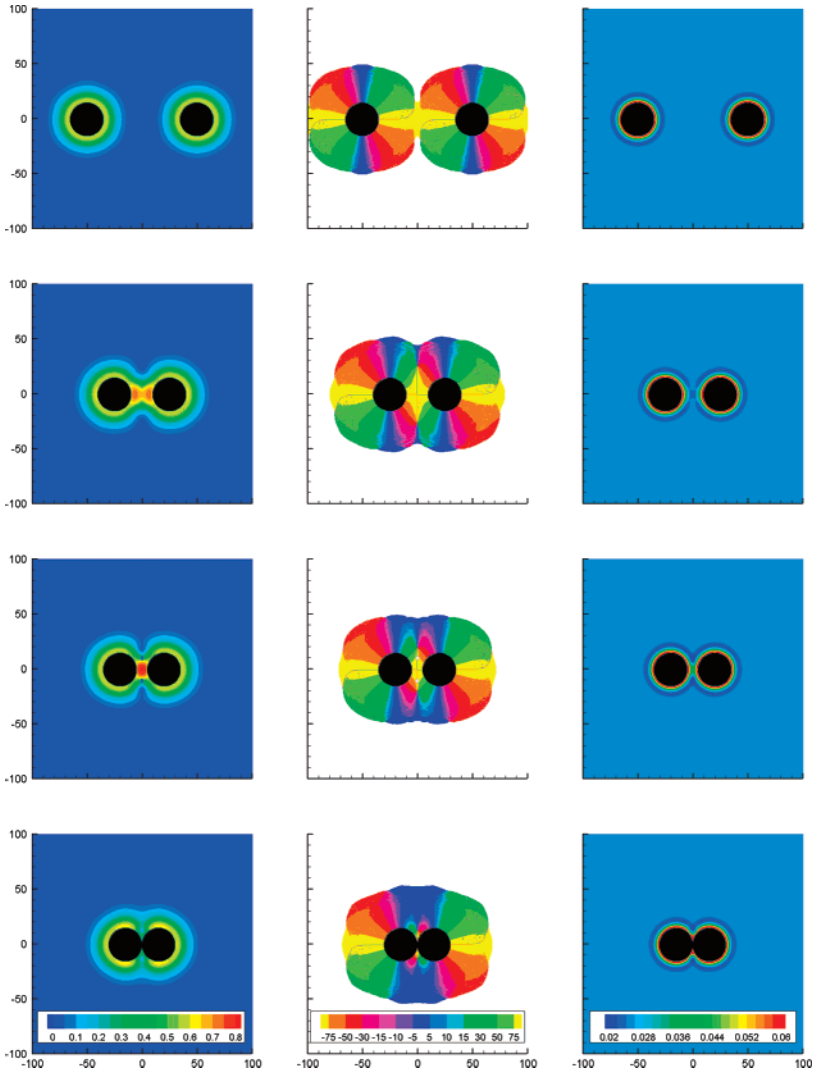

Figure 7. Maps of order parameter $Q(\boldsymbol{s})$ (left), director angle $\varphi(\boldsymbol{s})$ (center), and number density $\rho(\boldsymbol{r})$ (right) of liquid in the isotropic phase ($\beta\mu = 1.2$) around two cylindrical nanoparticles. Only the central region $-100 \le x/b, z/b \le 100$ is shown. The director map is only shown for values of the order parameter $Q(\boldsymbol{s}) > 0.001$.

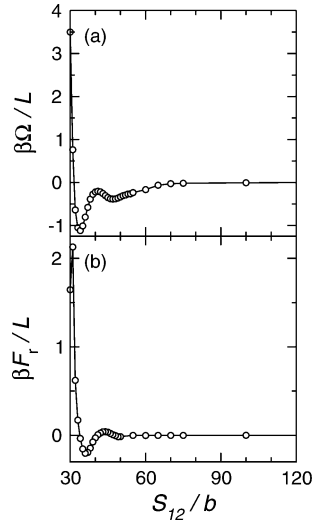

Figure 8. (a) Grand potential (per unit length) against separation for cylinders in the isotropic phase ($\beta\mu = 1.2$). (b) Radial force per unit length against separation for cylinders in the solvent isotropic phase.

This is consistent with previous theoretical work,[30] where for decreasing particle size the bridging transition changes from abrupt to continuous. The radial force F_r is also shown in Figure 8; it is similar in appearance to that seen in the nematic phase. The transverse force F_t is zero by symmetry.

4. Conclusions

Classical DFT within the Onsager second-virial approximation has been used to investigate the solvent-induced interaction between two cylinders suspended in an isotropic liquid and a nematic liquid crystal. The interactions in the two phases are qualitatively different. In the nematic phase, the interaction is highly anisotropic and gives rise to a component of force perpendicular to the cylinder−cylinder separation vector. For the separations considered in this work, the interaction is found not to be quadrupolar, in agreement with MD simulations and phenomenological theory.[26] In the isotropic phase, close to the NI transition, the formation of a nematic bridge between the cylinders gives rise to an attractive interaction.

Acknowledgment. This research was supported by EPSRC Grant GR/S77240. The calculations were performed at the computing facilities of the Centre for Scientific Computing, University of Warwick.

LA702348C

(30) Stark, H.; Fukuda, J.; Yokoyama, H. *Phys. Rev. Lett.* **2004**, *92*, 205502/1−4.